Plasma Sources Sci. Technol. **7** (1998) 268–281. Printed in the UK PII: S0963-0252(98)94214-1

Fast modelling of low-pressure radio-frequency collisional capacitively coupled discharge and investigation of the formation of a non-Maxwellian electron distribution function

S V Berezhnoi†, I D Kaganovich†‡ and L D Tsendin†

† Physical Technical Department, St Petersburg State Technical University, 195251, Russia
‡ University of Antwerpen, Department of Chemistry, Universiteitsplein 1, B-2610 Wilrijk, Belgium

Received 11 August 1997, in final form 12 February 1998

Abstract. The principles of fast modelling (FM) of a low-pressure radio-frequency capacitively coupled discharge are presented. They are based on averaging over fast electron and ion motions and on eliminating a small spatial scale, the Debye radius. As a result, the solution of a self-consistent system of the electron kinetic equation, Poisson and ion continuity equations takes approximately 10 min on a 486 PC. The calculation of discharge parameters has been performed for a wide range of current and pressure. The comparison with full-scale Monte Carlo calculations and experimental data has been performed. The performed comparisons demonstrate that the developed method of fast modelling has a good accuracy for calculating the global parameters such as central plasma density, applied voltage, sheath thickness, ionization rate, etc, and the profiles of plasma density and the electric fields. The accuracy of the electron distribution function (EDF) calculation is high when the EDF form is not enriched by slow electrons, and seems satisfactory in the case of a strongly peaked EDF. The results are in qualitatively good agreement with the experiment. The quantitative agreement is mainly within a factor of two. This discrepancy can be attributed to the fact that the EDF form is very sensitive to the details of plasma description, e.g. small variation of cross-sections results in considerable changes in the EDF. The mechanism of non-Maxwellian EDF formation due to non-locality effects has been analysed. The evolution of the low-pressure radio-frequency collisional capacitively coupled discharge with current and pressure variation has been investigated.

1. Introduction

Radio-frequency (RF) capacitively coupled plasma (CCP) is widely used in the plasma aided materials processing industry: in deposition, etching, etc. The interest in study of the CCP has been also invoked by the interesting physical phenomenon of formation of the strongly non-Maxwellian electron distribution function (EDF) which is inherent to this type of discharge.

These facts make it absolutely necessary to use rigorous kinetic description of electrons even for a qualitative description of low-pressure CCP. The form of EDF is influenced by many processes and strongly depends on discharge conditions. It means that the global models [1] accounting for only simple forms of EDF, which are similar over the whole discharge gap, are of restricted and uncontrollable accuracy.

The concave shaped EDF with a strongly pronounced group of low-energy electrons was observed in the CCP [2]. The mechanisms of formation of the non-Maxwellian EDF have been discussed in [3]. It is difficult to analyse the complex self-consistent structure of the CCP without a corresponding numerical simulation. Thus, there has been a substantial effort in recent years to model these systems self-consistently. However, the existing types of simulation are computationally very expensive. This does not allow us to perform calculations in a wide range of parameters, to obtain scaling laws, and to predict

0963-0252/98/030268+14$19.50

the dependence of the internal plasma parameters on the externally controllable factors such as pressure, current, frequency, etc. The possibility of a serious reduction of the computational work in the discharge modelling implies an optimal combination of numerical and analytic approaches. In application to the CCP the analytic approaches have been developed and reported earlier [3]. They consist in averaging over the fast plasma motions, in eliminating the small spatial scales and in the division of the whole discharge volume into the quasineutral plasma region and space-charge sheaths [3]. The numerical integration of the resulting reduced system is considerably simpler than the straightforward modelling and also more physically transparent. Another serious advantage of such a semi-analytic or fast modelling procedure, with respect to the standard one, which comprises numerical investigation of the Boltzmann and Maxwell equations, is the possibility to trace explicitly the influence of different physical mechanisms and to achieve understanding of the underlying physics. Since the accuracy of the analytic procedure is easy to estimate, with such a strategy we can avoid unnecessary computational work and in every case single out only the dominant physical mechanisms.

Such a program was implemented for the inductive coupled low-pressure RF plasma (ICP) in [4], and for the dc positive column in [5]. User-friendly PC-oriented compact programs were developed which enabled us to perform fast self-consistent kinetic analysis, to obtain scaling laws, to understand basic physical mechanisms, etc. For the case of CCP, the problem turned out to be considerably more complicated than in ICP or a positive column. One of the central problems is related to the structure of an electric field. In the dc positive column a strict distinction exists between a uniform field along the tube axis which induces the current and heats electrons, and a radial ambipolar field which restricts electrons trapped in the plasma bulk and does not perform work over electron gas. In case of the ICP [4], an ambipolar field is directed normally to the plasma boundary, and the RF inductive field is tangential to it. Both these factors, combined with the evidence that the boundary of the quasineutral plasma is fixed, greatly simplified analysis in [4]. In the CCP, even for the simplest 1D geometry, this boundary moves in a rather complicated way; the quasineutrality of the plasma, and its heating (both Joule and stochastic [6]) are provided by the 1D electric field.

This paper is organized as follows. Section 2 describes in detail the system of equations for the fast modelling (FM). In order to demonstrate explicitly the advantages of the FM method, we restricted ourselves in this paper to the simplest collisional non-local situation, when the particle mean free path is small with respect to both the discharge gap and the sheath thickness, and the collisionless electron heating is small. In the developed framework this effect as well as deviations from non-locality, influence of the γ-electrons, etc, can be easily accounted for. In section 3 the validity of the FM is checked by comparison of the results with previously reported data obtained by the full-scale modelling. Section 4 presents analysis of the experimental data of [7] with the use of the FM. The results of the investigation of system evolution with current and pressure variation are presented. The effects of the non-locality, of the Ramsauer minimum, and electron–electron collisions on the formation of a low-energy EDF peak are studied. In section 5, it is demonstrated that the form of EDF is very sensitive to the different processes, e.g. if small corrections in cross-sections are taken into account it will result in considerable change in the EDF. Section 6 contains the conclusions and outlook.

2. Principles of fast self-consistent kinetic modelling of low-pressure collisional capacitively coupled RF discharge

For simplicity a planar symmetric geometry is considered, but the theory can be easily generalized and extended to more complicated systems. We consider the RF capacitively coupled discharge at low pressures in the collision-dominated regime 0.01 Torr $\lesssim$ 0.1 Torr. A sketch of the RFC discharge is presented in figure 1(a). A sketch of the plasma–sheath boundary motion and the region of the electron motion is presented in figure 1(b).

The EDF in the CCP is typically far from Maxwellian. Therefore the EDF is to be obtained from the Boltzmann kinetic equation or from straightforward particle simulation. The time varying electric field maintaining the discharge should be found by solving the Poisson equation or from the quasineutrality condition. The ion density profile is governed by the continuity equation. A full description of the CCP is given by a complex self-consistent system of non-linear non-stationary equations including the electron kinetic equation, Poisson equation and ion continuity equation.

The attempts to solve this system in a straightforward way without any simplification meet with numerical difficulties, since simulations of this kind are very time and resource consuming. Because of this it is difficult to perform calculations in a wide range of discharge parameters and to deduce understanding of the underlying complicated physics. The main source of computational difficulties lies in the fact that temporal and spatial scales to be resolved differ quite drastically.

The largest characteristic frequency is the electron plasma frequency ω_{0e}. The minimal frequency is the frequency of ion escape from the plasma bulk which is of the order of D_a/L_0^2, where D_a is the ambipolar diffusion coefficient, and L_0 is half of the discharge gap. For example, for the plasma density $n = 10^9$ cm^{-3}, and $\omega_{0e} = 1.7 \times 10^9$ s^{-1}. For argon, at pressure $P = 0.01$ Torr, $L_0 = 3$ cm and electron temperature $T_e = 3$ eV, the frequency of ion escape is $\sim 3 \times 10^4$ s^{-1}. Thus, the ratio of the maximal and the minimal characteristic frequency constitutes five orders of magnitude.

The characteristic spatial scales in Poisson equation are the Debye radius r_D, sheath length L_{sh} and L_0. For $n = 10^9$ cm^{-3}, and $T_e = 3$ eV, the Debye radius is 0.3 mm. The sheath length is typically about 1 cm, and L_0 is in the range 2–10 cm. The ratio of L_{sh} or L_0 to r_D is very considerable.

The value of electric field can vary from $\sim$1 kV cm^{-1} in the region of ionic space charge (ISC) to $\sim$1 V cm^{-1} in the plasma bulk. The ion density profile in the sheath is determined by the ISC intense field, and the electron distribution function is determined by the weak field in the plasma bulk. To calculate both these important characteristics with reasonable accuracy, the electric field must be simulated with accuracy higher than 0.1%.

The equation system for the FM derived in [3] makes it possible to overcome the above mentioned difficulties.

2.1. Separation of discharge space into plasma and ionic space charge region

To eliminate the small spatial scales, we assume from the beginning that the whole discharge volume could be divided into two regions: the region of quasineutral plasma, where $n_e \cong n_i$, and the region of ionic space charge $n_e \leq n_i$. The quasineutrality condition $n_e \cong n_i$ in the plasma bulk is valid, if the electron plasma frequency satisfies the inequality

$$\omega_{0e} \gg \max(\sqrt{\nu\omega}, \omega) \tag{1}$$

ν being the electron–neutral collision frequency, and the Debye radius is assumed to be small compared with the discharge gap [8]. These conditions are fulfilled for rather wide range of plasma parameters: $\omega \sim 10$ MHz, $n > 10^8$ cm^{-3} ($n \sim 10^9$ cm^{-3}) and $T_e \sim 3$ eV.

The applied RF voltage U (10–1000 V) is screened by the ionic space charge (ISC) at the plasma periphery (in the sheath region). Usually, the amplitude of applied voltage is much larger than the electron temperature (divided by electron charge). Therefore, in the ISC region $n_e \ll n_i$. The width of the transitional region between the plasma and ISC, where n_e is comparable with n_i, is of the order of the r_D. Since $U \gg T_e/e$, the Debye radius is small in comparison with the sheath thickness $L_{sh} \sim r_D\sqrt{eU/T_e}$ [9]. This inequality allows one to use the concept of a sharp boundary between the plasma and the ISC [1, 10]. The potential drop between plasma and electrode changes with time. Consequently, the sharp boundary between plasma and ISC will be oscillating due to the alternation of $U(t)$. The movement of the boundary coincides with an average electron motion at the edge of the plasma [8]. The region occupied by the plasma oscillates between the electrodes and at some moments practically will be in contact with them. At any point of the sheath (within $L_p < |x| < L_0$, figure 1(a)) the whole field period is to be divided into two parts. During the first part the electrons are absent, and the ionic space charge phase occurs ($t_1 < t < t_2$, figure 1(b)), during the second part of period the ionic space charge phase is replaced by the plasma phase $t_2 < t < t_3$; at the points where and at the moments when electrons are actually present the condition $n_e \cong n_i$ holds. The plasma–ISC boundary motion as a function of $Z \equiv \omega t$ corresponds to the curves $X_{1,2}(\omega t)$ (see figure 1(b)). In coordinates $\{x, t\}$, the plasma phase corresponds to the single-hatched region (see figure 1(b)).

2.2. Separation of electric field into different parts

The electric field strength in the ISC is very high, being of the order of 1 kV cm^{-1}. In the plasma bulk it is considerably lower—of the order of 1 V cm^{-1}. Hence the ion motion in the sheath is determined by the high field in the ISC phase, and the electrons are only subject to the weak plasma field. This means that both these fields are to be known accurately, and it is natural to consider these electric fields in ISC and plasma independently. This can be done using the concept of a sharp boundary between plasma and ISC. Since the total current (the conductivity plus displacement ones) is spatially uniform in the 1D plane-parallel geometry, the simplest configuration of the external circuit corresponds to the current generator. The total current $j(t) = -j_0 \sin(\omega t)$ is transported in the ISC in the form of a displacement current $(\partial E/\partial t)/(4\pi)$. It follows that $E(x, t) = (4\pi j_0/\omega)(\cos(\omega t) + A(x))$; the arbitrary function $A(x)$ should be found from the condition that this large electric field should be almost totally screened at the plasma–ISC moving boundary $X_{1,2}(\omega t)$. Introducing the phase $Z_{1,2}(x)$ as the *one-valued* inverse functions of $X_{1,2}(\omega t)$, the expression for ISC electric field can be rewritten in the form [8, 11, 12]

$$E(x, t) = \frac{4\pi j_0}{\omega}(\cos(\omega t) - \cos(Z_{1,2}(x))). \tag{2}$$

For a wide range of plasma parameters ($\omega \sim 10$ MHz, $n < 10^{11}$ cm^{-3}) the inequality

$$\omega_{0i} \ll \sqrt{\nu_i \omega} \tag{3}$$

is valid where ω_{0i} is an ion plasma frequency and ν_i is an ion–neutral collision frequency. Consequently, the ion displacement during the RF field period is small with respect to the sheath thickness $L_{sh} = L_0 - L_p$; so during this short time the ion density profile can be considered as stationary [1, 10].

Substituting (2) into the Poisson equation $\partial E(x, t)/\partial x = 4\pi e n_i(x)$ yields the following equation for the plasma–ISC boundary position $Z(x)$

$$\frac{\mathrm{d}Z}{\mathrm{d}x}\sin(Z) = \frac{e\omega n_i}{j_0}. \tag{4}$$

Since the inequality (1) holds, the total current in the plasma coincides with electron current [8]

$$j(t) = \sigma E(x, t) + eD\frac{\mathrm{d}n}{\mathrm{d}x} \tag{5}$$

where σ is the electron conductivity†, D is the electron diffusion coefficient.

The electric field in the plasma ($|x| < L_p$) and in the plasma phase in the sheath can be divided into an oscillatory part $\tilde{E}(x, t)$, and a dc part $\overline{E}(x)$ (time averaged part) as follows

$$E(x, t) = \tilde{E}(x, t) + \overline{E}(x). \tag{6a}$$

† Under our conditions $\lambda_\varepsilon \ll L_{sh}$ spatial dispersion in conductivity can be neglected. The expression for conductivity for the general case was derived in [13–15].

Here $\overline{E}(x)$ is determined by

$$\overline{E}(x) = \frac{\omega}{2\pi}\int_0^{2\pi/\omega} E(x,t)\,\mathrm{d}t \equiv -\frac{\mathrm{d}\Phi}{\mathrm{d}x}. \qquad (6b)$$

From equation (5) the expressions for $\tilde{E}(x,t)$, and $\overline{E}(x)$ can be obtained

$$j(t) = \sigma\tilde{E}(x,t) \qquad (7)$$

$$\sigma\overline{E}(x) = eD\frac{\mathrm{d}n_i}{\mathrm{d}x} = 0. \qquad (8)$$

In (8), the quasineutrality condition $n_e = n_i(x)$ was used.

From equation (7) it follows that $\tilde{E}(x,t)$ accounts for the ordinary ohmic heating. The stationary ambipolar field $\overline{E}(x)$ extracts the ions from plasma and traps the electrons in the plasma bulk. It does not perform work over electrons, since the time averaged electron current $\langle j\rangle$ is practically zero ($\langle j\rangle\overline{E}(x) = 0$). Actually it is equal to the small ion current.

In order to solve the electron kinetic equation it is necessary to know only the field in the plasma phase. In the sheath it corresponds to the time interval $(t_3 - t_2)$ (single-hatched region in figure 1(b)). The proposed field division in the plasma phase in the sheath is represented by

$$E(x,t) = \tilde{E}(x,t) + \overline{E}(x)$$

$$\overline{E}(x) = \frac{1}{t_3 - t_2}\int_{t_2}^{t_3} E(x,t)\,\mathrm{d}t \equiv -\frac{\mathrm{d}\Phi}{\mathrm{d}x}. \qquad (9)$$

The proposed field division was also implemented in 'usual' MC simulations in [16], which enabled the authors to considerably speed up their calculations.

2.3. Ion motion

The ion continuity equation reads:

$$\frac{\partial n_i}{\partial t} + \frac{\partial n_i u_i}{\partial x} = I(x,t) \qquad (10)$$

where $I(x,t)$ is an ionization rate. In the validity domain of (3) the ion density profile is stationary $n_i(x)$ and is governed by (10) averaged over the RF period as follows

$$\frac{\partial n_i\langle u_i\rangle}{\partial x} = \langle I(x,t)\rangle \qquad (11)$$

where angular brackets denote time averaging over the whole discharge period.

We consider the collision dominated regime when the ion mean free path λ_i is small in comparison with L_{sh}, L_0. The ion kinetic equation reads

$$\frac{\partial f}{\partial t} + eE(x,t)\frac{\partial f}{\partial v} = -\nu_i(v)f. \qquad (12)$$

For low pressure ($p < 0.1$ Torr) the inequality $\omega \gg \nu_i$ holds. It yields that the ion distribution function f is almost stationary and can be found from the time averaged equation (12):

$$e\langle E(x,t)\rangle\frac{\partial f}{\partial v} = -\nu_i(v)f. \qquad (13)$$

For the ion–neutral elastic cross section taken in the form $\sigma_{ia} = \sigma_0 v^\beta$, $-1 \le \beta \le 0$, equation (13) can be solved, and the resulting ion mean velocity takes the form

$$u_i = \pm\left(\frac{4e(\beta+2)}{MNa\sigma_0}\right)^{1/(2+\beta)}\frac{1}{2\sqrt{\pi}}\Gamma\left(\frac{4+\beta}{2(2+\beta)}\right) \times|\langle E(x,t)\rangle|^{1/(2+\beta)} \qquad (14)$$

where Γ is the gamma function. Here the plus sign corresponds to the right sheath, minus to the left one. This approximation corresponds to the Monte Carlo calculations of [17, 18] (see 3.1, 3.2). The real dependence of ion mobility on $\langle E\rangle$ is more complicated than the power approximation (14). In section 5 this problem is considered in more detail.

According to the proposed field division, the average electric field in the sheath includes the ambipolar field averaged over the plasma phase $-(\mathrm{d}\Phi(x)/\mathrm{d}x)$, and the field averaged over the ISC phase (2)

$$\langle E(x,t)\rangle = -\frac{\mathrm{d}\Phi}{\mathrm{d}x}(1 - Z(x)/\pi) \pm\frac{4j_0}{\omega}[\sin(Z(x)) - Z(x)\cos(Z(x))]. \qquad (15)$$

In the plasma bulk, $Z = 0$ and the averaged electric field and the ambipolar field coincide with each other.

2.4. The electron kinetic equation

Since the EDF in the CCP is typically far from Maxwellian, EDF is to be found from the Boltzmann kinetic equation.

We consider the RF capacitively coupled discharge, when the energy relaxation length λ_ε exceeds L_0. As a rule, the energy relaxation length is of the smallest magnitude at the EDF tail. Accordingly, the energy relaxation length can be estimated as $\lambda_\varepsilon \sim \sqrt{\lambda\lambda^*/3}$ at the EDF tail (λ^* is a mean free path for inelastic collisions). For example, the condition $\sqrt{\lambda\lambda^*/3} > L_0$ demands $pL_0 < 0.4$ Torr cm for helium, and $pL_0 < 0.1$ Torr cm for argon. This corresponds to strong non-locality, when the form of the EDF is determined by the whole profile of the electric field.

We restrict ourselves to the collision dominated case, when both L_0 and L_{sh} greatly exceed the electron mean free path λ_c. The generalization is possible for the opposite case as well. The expression for conductivity and diffusion coefficient in energy space was derived in [13–15] and a model calculation with account of collisionless heating was performed in [19]. It follows that the contribution of the so-called stochastic electron heating to the electron kinetic equation at $\lambda_\varepsilon \ll L_{sh}$ is negligible [6]. Hence, the two-term approximation $f(x,\boldsymbol{v},t) = f_0(v,x,t) + f_1(v,x,t)\cos(\theta)$ is valid, where θ is the angle between the direction of plasma density gradient which coincides with the direction of the electric field and an electron velocity $\boldsymbol{v}$. The anisotropic part of the EDF f_1 is small compared with its isotropic part f_0 ($f_1 \ll f_0$) when inequality $\nu \gg \nu^*$ holds, where ν is a transport electron collision frequency, and ν^* is an inelastic collision frequency [20]. For noble gases, $\nu/\nu^* \sim 10^{-1}$–10^{-2} and $f_1 \ll f_0$.

Equations for f_0 and f_1 are well known [21]. The equation for the anisotropic EDF part is

$$\frac{\partial f_1}{\partial t} + \nu f_1 = -\frac{eE}{m}\frac{\partial f_0}{\partial v} - v\frac{\partial f_0}{\partial x}.$$

The equation for the isotropic part of the EDF is rather complicated

$$\frac{\partial f_0}{\partial t}+\frac{v}{3}\frac{\partial}{\partial x}f_1+\frac{e}{3mv^2}\frac{\partial}{\partial v}(v^2Ef_1)=\frac{1}{2v^2}\frac{\partial}{\partial v}\left(v^3\frac{2m}{M}\nu f_0\right)-\sum_k\left(\nu_k^*(v)f_0(u)-\nu_k^*(u+\varepsilon_k)\sqrt{1+\frac{\varepsilon_k}{u}}f_0(u+\varepsilon_k)\right).$$

Because of the suggested field division (6), (9) allows us to introduce a new variable—the total electron energy may be introduced $\varepsilon = mv^2/2 + e\Phi(x)$ [3]. When λ_ε exceeds L_0, the total electron energy is practically conserved during an electron displacement over the available region between the turning points $X_-(\varepsilon,t)$, $X_+(\varepsilon,t)$ (the double-hatched region in figure 1(b)). The plasma–ISC boundary corresponds to the rigid potential 'wall', which specularly reflects the electrons (see figure 1(b)). We assume that the discharge frequency satisfies the condition $\omega \gg \nu^*$. Therefore, the isotropic part of the EDF is practically stationary [22]. When the conditions $\omega \gg \nu^*$ and $\lambda_\varepsilon \gg L_0$ are applicable, the EDF satisfies $f_0(\varepsilon,x,t) \approx F_0(\varepsilon)$.

In other words, the assumption that the EDF depends solely on a total electron energy ε proves to be suitable for adequately accurate description of the electron kinetics. In comparison to $F_0(\varepsilon)$, the time- and coordinate-dependent parts of the EDF are small corrections of the order of (ν^*/ω), $(L_0/\lambda_\varepsilon)^2$; these approximations were checked theoretically [20, 22], experimentally [23] and numerically [24, 25].

The function $F_0(\varepsilon)$ is to be calculated from the spatially and temporally averaged kinetic equation [3]

$$\frac{\mathrm{d}}{\mathrm{d}\varepsilon}\left(\overline{vD_\varepsilon}(\varepsilon)\frac{\mathrm{d}F_0(\varepsilon)}{\mathrm{d}\varepsilon}+\overline{vV}_\varepsilon(\varepsilon)F_0(\varepsilon)\right)=\sum_k\overline{v\nu_k^*}(\varepsilon)F_0(\varepsilon)-\sum_k\overline{v\nu_k^*}(\varepsilon+\varepsilon_k^*)F_0(\varepsilon+\varepsilon_k^*) \tag{16}$$

where the electron energy diffusion coefficient (EEDC) is given by

$$vD_\varepsilon(v,x,t)=\cos^2 Z(x)e^2v^3\tilde{E}^2(x,t)\nu/(3(\omega^2+\nu^2)) \tag{17a}$$

and the electron energy losses vV_ε in elastic collisions are given by

$$vV_\varepsilon(v,x,t)=(m/M)mv^3\nu. \tag{17b}$$

Here ν, ν_k^* are elastic transport and inelastic collision frequencies, respectively; ε_k^* is an inelastic collision threshold. The space–time averaging is to be performed as follows

$$\overline{G(v,x,t)}\equiv\overline{G}(\varepsilon)=\frac{1}{2L_0T}\int_0^T\mathrm{d}t\int_{X_-(\varepsilon,t)}^{X_+(\varepsilon,t)}G\left(\sqrt{\frac{2}{m}[\varepsilon-e\Phi(x)]},x\right)\mathrm{d}x. \tag{18}$$

The electron kinetic equation (16) accounts for the heating of electrons in the RF electric field and for the inelastic and elastic energy losses.

It follows from equations (16)–(18) that the main characteristics of the electron kinetics are described by the function $\overline{vD_\varepsilon}(\varepsilon)$ which is an electron energy diffusion coefficient, temporally and spatially averaged over the RF period and over the area available for the electron with total energy ε†. In the energy interval $T^* < \varepsilon < \varepsilon_1$, where ε_1 is the first excitation potential, and $T^* = 1/(\mathrm{d}\ln F_0/\mathrm{d}\varepsilon)$ is an effective temperature at the EDF tail, where the inelastic collisions will occur, the right-hand side of equation (16) will vanish. Thus the solution of equation (16) will be simple:

$$F_0(\varepsilon)=\Gamma_\varepsilon\int_{\varepsilon 1}^{\varepsilon}\frac{\mathrm{d}\varepsilon'}{\overline{vD_\varepsilon}(\varepsilon')}. \tag{19}$$

This means that the EDF corresponds to conservation of the diffusive flux Γ_ε in the energy space.

There are several mechanisms which cause steep increase of $\overline{vD_\varepsilon}(\varepsilon)$ with ε. First, the available area increases with ε due to the fact that $\Phi(x)$ restricts the electron motion and becomes large with x. The second reason (see equation (17*a*)) is related to the fact that the ratio $v^3\nu/(\omega^2+v^2)$ usually is increasing with velocity. The most pronounced dependence is connected to the spatial dependence of the oscillatory field $\tilde{E}(x,t)$. Since the plasma density decreases towards the periphery, the field $\tilde{E}$ will be increasing with x. It means that electrons with higher ε, for which the available volume is large, 'feel' higher oscillatory field, and higher ohmic heating. This mechanism is especially effective for energies $\varepsilon > e\Phi_{sh} = e\Phi(L_p)$ corresponding to the ability of the electrons to penetrate into the sheath region. Since the ion density in the sheath is low, the oscillatory field in the plasma phase is high, when the electrons are present in the sheath. Figure 1(c) demonstrates the process of the EDF formation.

In the analysis presented in this paper, we omitted for simplicity the stochastic electron heating which results from collisions of electrons with the moving plasma–ion–space charge boundary [26]. The corresponding expressions were presented in [6]. Since the velocity of this boundary coincides with the electron drift velocity, in our case of collisional sheath, $(L_0 - L_p) > \lambda_\varepsilon$, the contribution of this mechanism is small.

The influence of non-homogeneity of plasma density on the EDF peak formation is analysed and illustrated in section 4.3.

2.5. The full self-consistent system of equations

To obtain a complete set of equations for the CCP, it is necessary to determine electron density, conductivity and ionization rate via the EDF

$$n_e(x)=\frac{4\pi}{m}\int_{e\Phi(x)}^{\infty}F_0(\varepsilon)\sqrt{\frac{2}{m}(\varepsilon-e\Phi(x))}\,\mathrm{d}\varepsilon \tag{20}$$

$$\sigma=-\frac{8\pi e^2}{3m^2}\int_{e\Phi(x)}^{\infty}v\frac{\varepsilon-e\Phi(x)}{\nu+\mathrm{i}\omega}\frac{\mathrm{d}F_0}{\mathrm{d}\varepsilon}\,\mathrm{d}\varepsilon \tag{21}$$

$$\langle I(x,t)\rangle=\left(1-\frac{Z(x)}{\pi}\right)\frac{4\pi\sqrt{2}}{m^{3/2}}\times\int_{e\Phi(x)+\varepsilon_1}^{\infty}[N_a v\sigma_{ion}(\varepsilon-e\Phi(x))]F_0(\varepsilon)\sqrt{\varepsilon-e\Phi(x)}\,\mathrm{d}\varepsilon \tag{22}$$

† The term $\overline{vV_\varepsilon}(\varepsilon)$ (17*b*) is usually small.

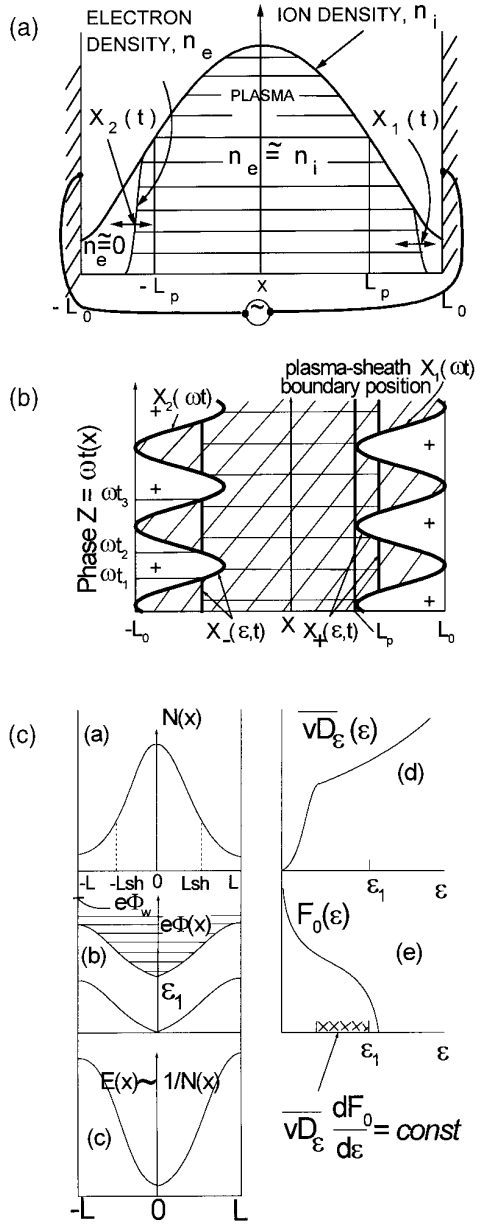

Figure 1. (a) Sketch of the RFC discharge. (b) Sketch of the plasma–sheath boundary motion (plasma region is single hatched) and sketch of the available region of the motion of an electron (double-hatched domain). (c) Sketch of the profiles of ion density (a), ambipolar potential (b), oscillatory field (c) and the corresponding electron energy diffusion coefficient (d) and the EDF (e). $e\Phi_W$ is the minimal wall potential at $Z = \pi$.

where N_a is neutral atom density, σ_{ion} is an ionization cross-section and ε_1 is an ionization threshold.

The quasineutrality condition determines the ambipolar potential:

$$\frac{4\pi}{m}\int_{e\Phi(x)}^{\infty} F_0(\varepsilon)\sqrt{\frac{2}{m}(\varepsilon - e\Phi(x))}\,\mathrm{d}\varepsilon = n_i(x). \qquad (23)$$

The boundary conditions $\Phi|_{x=0} = 0$, $(\mathrm{d}\Phi/\mathrm{d}x)|_{x=0} = 0$ follow from the system symmetry.

Thus, the self-consistent description of the CCP is completed. The full set of equations includes the electron kinetic equation (16), ion continuity equation (11) with the expression for ion mean velocity (14) and the source term in the form of equation (22), the Poisson equation in ISC (2), (4), the current conservation law takes the form of (7) in the plasma while the conductivity is given by equation (21), and the quasineutrality condition is represented by equation (23).

It should be noted that the field division proposed above allows us to avoid solving the Poisson equation in the plasma, which would have required a cumbersome calculation of small differences $(n_e(x,t) - n_i(x,t))$ with high accuracy.

Thus, the field division together with the approximation of the total energy conservation law are the key points of the non-local theory. By these particular assumptions the simulation of electron kinetics becomes fast.

2.6. Numerical method

The simulations have been performed according to figure 2.

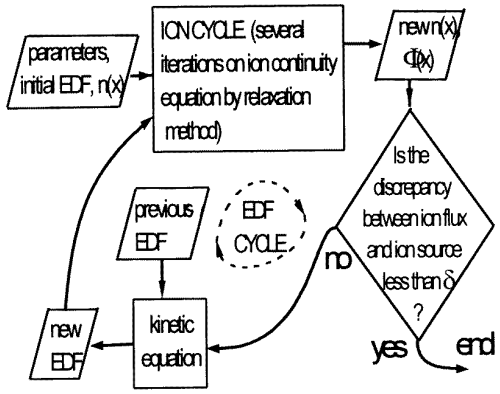

Figure 2. Flow chart of simulations.

The calculation starts from an initial EDF and an arbitrary ion density profile consideration. $\Phi(x)$ is obtained from equation (23). The 'ion cycle' corresponds to the solution of ion equation (11) by the relaxation method with fixed EDF. After several 'ion cycles' the new ion density profile and ambipolar potential are calculated. The calculation of the amplitude of the oscillatory field $\tilde{E}_0(x)$ is performed from equations (7), (21) the new $\Phi(x)$, $n_i(x)$ and the previous EDF. The new EDF is calculated from kinetic equation (16), with the new coefficients given by (17), (18). The 'EDF cycles' together with 'ion cycles' are repeated until steady state is reached.

The solution of the complete problem, which consists of calculation of the electron distribution, RF and stationary electric fields, and of the plasma density profile, for a simple atomic gas takes ~10 min on the IBM PC 486DX2/66.

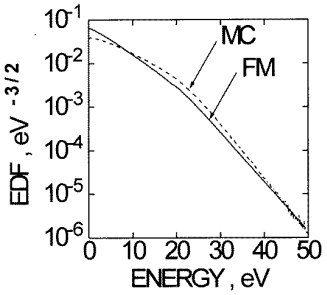

Figure 3. Comparison between EDF calculated in the non-local approach (marked as FM) and by Monte Carlo technique (marked as MC).

3. Verification of validity of FM by comparison with the full-scale modelling

To check the validity of the non-local approach and the method of field division a number of simulations have been performed†.

3.1. Verification of the procedure of field division and of the non-local approximation for the EDF

As the first step, we have checked the validity of the non-local approximation (16) and validity of the field division (6)–(9) [27]. In this simulation, we have restricted ourselves to the case of fixed ion density profile ($n_i(x) = 5\times10^8[1.0+0.075x-0.026x^2+0.214x^3+0.0705x^4]$ cm^{-3}; x in cm). Simultaneously with the FM, both the Poisson equation and electron kinetic equation have been solved self-consistently using a Monte Carlo (MC) techniques. Inelastic collisions were described only by excitation helium cross section $0.41 \times 10^{-17}(u - \varepsilon^*)$ cm^2 eV^{-1} (a threshold energy $\varepsilon^* = 20$ eV has been introduced). Assuming that the elastic collision frequency is independent of energy it was found to be 5×10^8 s^{-1}. A set of following discharge parameters for the MC simulation was introduced: applied voltage -62 V, discharge frequency $\omega = 2\pi\times15\times10^6$ s^{-1}, $L_0 = 2$ cm, pressure $P = 0.01$ Torr. The resulting EDF calculated by MC actually did not exhibit any variation with time during the RF period, since the strong inequality $\omega \gg \nu^*$ holds. The obtained EDF is presented in figure 3, marked by 'MC'. The MC simulation is more convenient to perform for a fixed value of voltage. In the FM a fixed value of current density was used. For this reason the value of current density $j_0 = 0.35$ mA cm^{-2} given by the MC simulation (applied voltage -62 V) was used for FM, as well. For the sake of comparison the EDF values calculated by both FM and MC methods are presented jointly in figure 3. The agreement between FM and MC EDF seems satisfactory. The difference of about 50% can be regarded as small because the EDF variation is of the order of 10^5.

Values of all the electric fields obtained by FM prove to be in reasonable agreement with the full-scale modelling. In the MC simulation the electric field $E(x,t)$ has been calculated directly from the Poisson equation for a discharge voltage $V(t) = V_0\sin(\omega t)$. Then the time-averaged part of the electric field and Fourier harmonics which are proportional to $\sin\omega t$ and $\cos\omega t$, $\tilde{E}_{sin}(x)$, $\tilde{E}_{cos}(x)$, of the RF field have been calculated in the MC simulation. The amplitude of oscillatory field $\tilde{E}(x,t)$ given by the MC simulation corresponds to $\tilde{E}_0(x) = \sqrt{(\tilde{E}_{sin}(x))^2 + (\tilde{E}_{cos}(x))^2}$ in the plasma ($|x| < L_p$). The values obtained differ from those calculated by FM (7) less than 25%. The difference between the time-averaged part of the RF field obtained by MC, and the gradient of the potential obtained by FM from equation (23) does not exceed 5% (comparison has been made in the plasma region ($|x| < L_p$). The discharge RF voltage is determined mainly by the strong ion space charge field. The resulting amplitude of applied voltage obtained by FM is in agreement with that utilized in the MC (relative difference is about $\sim$10%). Thus we can conclude that the values of ionic space charge field obtained by FM and MC simulations are in agreement, too. The difference in voltage values is of the order of electron temperature; it can be attributed to a zero Debye radius approximation used in the FM. Thus, the suggested division of electric field into three independent parts—the dc and oscillatory fields in the plasma phase and strong field in the ionic space charge phase—proves to be reasonably grounded and efficient.

To check a non-local approximation, the EDFs at different spatial points have been calculated by MC. The non-local approximation means that all the functions $f_0(u,x,t)$ will coincide with one function $F_0(\varepsilon)$, as a function of total energy. To transform functions $f_0(u,x,t)$ to the functions of this new variable (total energy ε), each function is normalized with respect to density at the corresponding spatial points and is shifted along the energy axis by the plasma potential $e\Phi(x)$. To make comparison more evident, we have divided all the resulting functions by the EDF calculated by MC at the discharge centre (see figure 4). If these functions strictly correspond to one function which depends only upon the total energy, then these ratios are to be unity.

The deviation from unity of the resulting ratios is less than 20% up to energies $\approx$35–40 eV. This indicates that the EDF depends practically only on ε. Consequently, the non-local approximation for EDF is valid in our conditions. The value of energy relaxation length λ_ε is 2 cm for $\varepsilon = 30$ eV, and $L_p = 1$ cm. Thus, the accuracy of the non-local approach should be of the order of $(L_p/\lambda_\varepsilon)^2 \sim 0.25$. It corresponds to the obtained difference in EDF ratios $\leq 20\%$.

Another check [28] of the FM validity has been made by comparing the FM results with the results of independent full-scale simulation [17]. In this comparison we have also calculated only EDF using the fixed ion density profile from [17]. The particle-in-cell (PIC) method with Monte Carlo techniques was used in [17]. The model gas was based on helium. It is only the ionization with the ionization threshold $\varepsilon_I = 24.5$ eV that has been introduced in [17]. No other inelastic collisions have been considered. The discharge parameters were: pressure $P = 0.06$ Torr; applied voltage 800 V; $\omega = 2\pi \times 30 \times 10^6$ rad s^{-1};

† For the ion velocity the approximation (14) was used in 3.1, 3.2. The experimental data $U_{ion}(E/p)$ [11] were used instead of (14) to compare the results of FM to the experimental ones. Also see section 5.

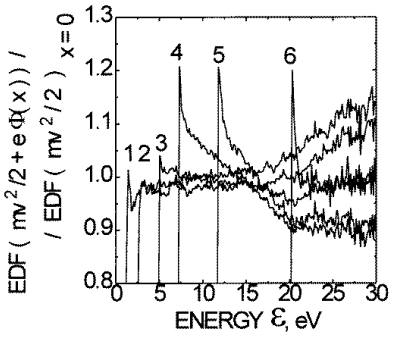

Figure 4. The ratios of the shifted (see text) EDFs calculated at different spatial points to the EDF calculated at the centre of the discharge: 1: x = 0.69 cm, 2: x = 1.0 cm, 3: x = 1.35 cm, 4: x = 1.5 cm, 5: x = 1.67 cm, 6: x = 1.84 cm. The EDF is zero at $\varepsilon < e\Phi(x)$.

and half the discharge gap $L_0 = 2$ cm. The electron–neutral transport cross-section was assumed to be of the following form: $\sigma_{eq}^{tr} = 1.7 \times 10^{-14}(1 - \ln(1+\varepsilon)/\varepsilon)/[(\varepsilon \times 10)^{1.1}\ln(1+\varepsilon)]$ cm^2, ionization cross-section was $\sigma^{ioniz} = 10^{-13}(\varepsilon - I)/[(\varepsilon+50)(\varepsilon+300)^{1.2}]$ cm^2. Here the energy ε is in eV. The energy of electrons created by electron impact ionization was distributed according to the probability distribution function $S(W, P) = \{B\sigma_{ion}(W)/\tan^{-1}[(W - \varepsilon_I)/2/B]\}(P^2 + B^2)^{-1}$ [17], where W is the energy of the primary electron, P is the energy of the progeny electron, σ_{ion} is the ionization cross section. B is set to 10 eV. The averaged value of P is $\{B/2\tan^{-1}[(W - \varepsilon_I)/(2B)]\}\ln[((W - \varepsilon_I)/2B)^2 + 1]$. For the case of $(W - \varepsilon_I) < 2B$ we obtain $P \approx 1/4(w - \varepsilon_I)$, and for simplicity we set the energies of the progeny and primary electrons after ionizing collision equal to $1/4(W - \varepsilon_I)$ and $3/4(W - \varepsilon_I)$, respectively. In addition to ionization, it is necessary to account for the electrons arriving on electrodes (in our previous EDF calculation both processes were neglected in comparison to the excitation collisions). In the steady state, the number of escaped electrons is equal to the number of electrons created by ionization. Rigorously speaking, the wall escape of the fast electrons occurs at $\varepsilon > e\Phi_W$, where Φ_W is the minimal wall potential, figure 1(c). From the calculations for a positive column [29, 30] it follows that $e\Phi_W$ is of the order of the ionization energy. Hence, the simplest way to account roughly for the electron escape is to double the frequency of the loss of high-energy electrons in ionizing collisions. Finally, the right-hand side of the electron kinetic equation (16) reads

$$\overline{2v\nu^{ioniz}}(\varepsilon)F_0(\varepsilon) - 4[\overline{v\nu^{ioniz}}(4\varepsilon + \varepsilon_I)F_0(4\varepsilon + \varepsilon_I) + 1/3\overline{v\nu^{ioniz}}(4/3\varepsilon + \varepsilon_I)F_0(4/3\varepsilon + \varepsilon_I)]. \quad (24)$$

Under the assumed conditions the non-locality condition $(L_p/\lambda_\varepsilon)^2 < 1$ holds up to energies ≈100 eV.

The comparison between the EDF calculated in the non-local approach and by the Monte Carlo technique is presented in figure 5. The solid line in figure 5 corresponds to the EDF calculation by the MC method [17]; bars denote the variation of the EDF at the different phases of the RF field. In the region $\varepsilon \leq 25$ eV, EDF [17] does not exhibit any variation with time during the RF period.

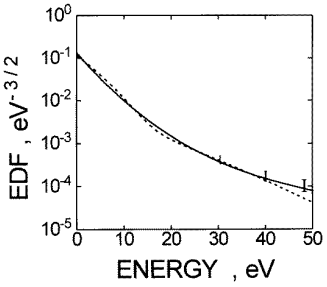

Figure 5. Comparison of the EDF calculated in the non-local approach with the EDF obtained by the Monte Carlo technique. The solid line corresponds to MC calculation [19]; the dashed line corresponds to the FM results. Bars denote the variation of the EDF at the different phases of the RF field.

The agreement between the EDFs calculated in the FM approach and by the Monte Carlo technique seems to be good.

3.2. Verification of the ion profile calculation and of the complete self-consistent FM procedure

Further check of the FM procedure employed the verification of the ion profile calculation and of the complete self-consistent FM procedure. Under conditions assumed in [17] (3.1), a complete FM gives a value of $N_0 = 5.5 \times 10^9$ cm^{-3} for the ion density at the discharge centre ($N_0 = 5.0 \times 10^9$ cm^{-3} in [17]), and 1.4 cm for the sheath thickness (1.2 cm in [17]), respectively.

We have also performed the complete self-consistent FM calculation for argon-like gas accounting for the Ramsauer minimum (in contrast to helium). The results obtained were compared with the full-scale simulation using the PIC method with Monte Carlo techniques [18]. The cross-sections used for simulation were taken from [18]. The excitation in the electron–atom collisions was not introduced. The distribution of the energy of electrons created by electron impact ionization used in [18] allows us to set the averaged energies of the progeny and primary electrons equal to $1/4(W - \varepsilon_I)$ and $3/4(W - \varepsilon_I)$, respectively. Accounting for the electron arriving on the electrodes, the right-hand side of the electron kinetic equation is the same as (24). The discharge parameters were: pressure $p = 0.05$ Torr; applied voltage 500 V; $\omega = 2\pi \times 12 \times 10^6$ rad s^{-1}; $L_0 = 2$ cm; the ion mass was 4 ae; the resulting current density from [18] which was used in FM calculations amounted to 2.3 mA cm^{-2}. This yields a value of 558 V for the FM voltage ∼10% different from the MC voltage.

For these conditions the criterion (3) is satisfied (the frequency of ion drift through the sheath $u_i/L_{sh} \sim 10^6$ is much smaller than $\omega \sim 10^8$ rad s^{-1}) so that the ion density profile is stationary. Under the conditions used the non-locality criterion $(L_p/\lambda_\varepsilon)^2 < 1$ will hold up to energies ≈100 eV. In figure 6, the resulting EDFs, the ionization rates and the ion density profiles of the full self-consistent FM and the MC calculations are presented.

In contrast to the He-like model, a strongly pronounced group of low-energy electrons was observed. It can be seen

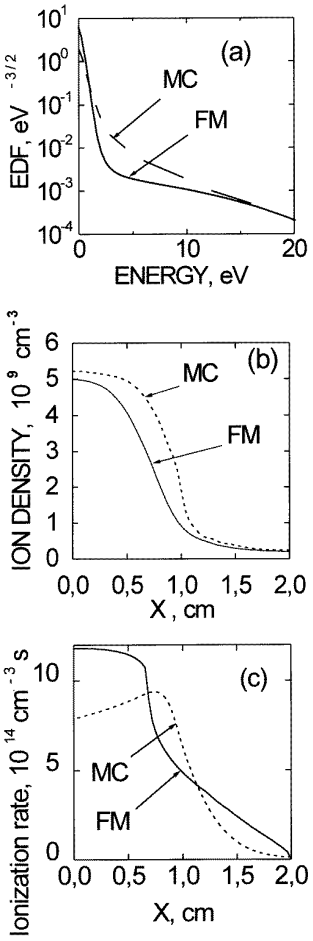

Figure 6. Comparison between results of the full self-consistent FM and the MC calculations for Ar-like gas. Solid line corresponds to the FM calculation, dashed lines correspond to the MC results [20]. (a) The EDFs; (b) the ion density profiles; (c) the ionization rates. Parameters are: p = 0.05 Torr; applied voltage 500 V; $\omega = 2\pi \times 12 \times 10^6$ rad s^{-1}; L_0 = 2 cm.

that the qualitative agreement between the EDFs is good. The quantitative agreement seems satisfactory. The ion density profiles calculated by both the FM and MC are close to each other. The ion density drop at the plasma–sheath boundary appears to be at smaller values of x for the FM. This is probably due to small values of ion mean free path ($\lambda_i \ll L_{sh}$) used in the FM approximation. Under the used conditions $\lambda_i = 0.4$ cm is comparable with $L_{sh} \sim 1$ cm. In equation (14), the ion velocity $u_i(x)$ is determined by local mean electric field in the sheath $\langle E(x,t)\rangle$. If we account for the finite ion mean free path, a spatial lag of the order of λ_i between $u_i(x)$ and $\langle E(x,t)\rangle$ will appear. As a result, the value of the ion velocity is smaller than that found from equation (14). Consequently, the plasma density drop would occur at larger values of x accounting for the spatial lag of the ion velocity. Thus, the difference in ion density profiles can be attributed to this effect.

The comparisons performed demonstrate that the developed method of FM proves to be of a good accuracy for the calculation of the plasma density and electric fields profiles, parameters including central plasma density, applied voltage, sheath thickness, ionization rate, etc. It provides far more detailed and accurate information than so-called global models that operate mainly with average parameters, with a given EDF. The accuracy of the EDF calculation is high when EDF is not enriched by slow electrons, and seems satisfactory in the case of the strongly peaked EDF.

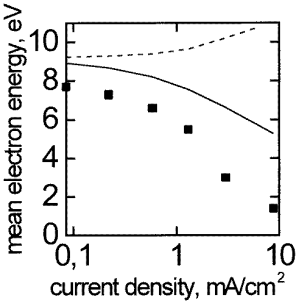

Figure 7. Mean electron energy versus current density. He, p = 0.1 Torr, ω = 13.56 MHz, L_0 = 3.35 cm. Experimental data—filled squares, the FM results—solid line. The dashed line corresponds to the results of FM when the Joule heating of the electrons in the sheath is not taken into account.

4. Analysis of experimental data

4.1. Comparison of the FM results with the experimental data in helium

Now we can apply the FM method to the simulations of discharges in real gases. First, we shall analyse the EDF formation in helium (He), considering it a gas lacking the Ramsauer minimum. The validity of the non-local approach demands $pL_0 \leq 0.4$ Torr cm. The measurements [7] were performed at $\omega = 13.56$ MHz, $L_0 = 3.35$ cm, $p = 0.1$ Torr. The FM calculations have been performed in a wide range of current densities and pressures: $j_0 = 0.085$–8.8 mA cm^{-2}, and $p = 0.03$–0.1 Torr. The values of cross-sections and ion mobility used in the FM were taken from [11].

The mean electron energy versus current density is presented in figure 7. The solid line corresponds to the FM results. The filled squares correspond to the experimental data. The discharge voltages versus current density are shown in figure 8. In figure 9 the experimental and calculated EEDFs at $j_0 = 0.085$, 0.22, 0.58, 1.3, 6.0, 8.8 mA cm^{-2} are plotted together.

In figure 10 (solid lines), the calculated EDFs at $j_0 = 0.085$, 0.22, 1.3, 6.0 mA cm^{-2} are shown. The data obtained demonstrate that the EDF peak can appear solely due to a non-locality effect. However, the calculated mean electron energy exceeds the experimental value approximately threefold at large currents (see figure 7). This difference can be attributed to the influence of γ-electrons. The estimates demonstrate that the γ-ionization can be noticeable under the used conditions. This problem demands separate investigation.

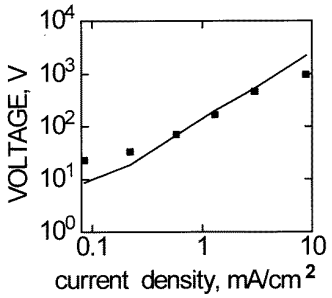

Figure 8. Discharge voltage versus current density. The experimental conditions are the same as in figure 7; FM—solid line, experimental data are represented by filled squares.

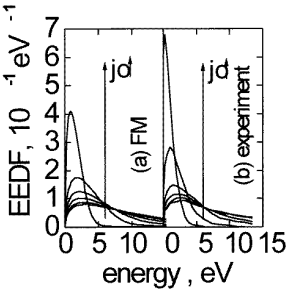

Figure 9. Calculated and experimental EEDFs in helium. The conditions are the same as in figure 7; j_0 = 0.085, 0.22, 0.58, 1.3, 6.0, 8.8 mA cm^{-2}. (a) The calculated EEDFs; (b) the experimental EEDFs.

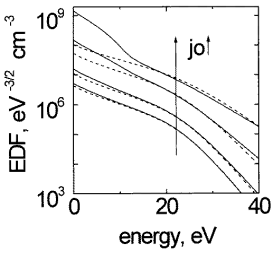

Figure 10. Calculated EDFs in helium. The conditions are the same as in figure 7; j_0 = 0.085, 0.22, 1.3, 6.0 mA cm^{-2}. Solid lines correspond to the results of FM. The dashed lines correspond to the results of FM, when the Joule heating of the electrons in the sheath is not taken into account.

The simulations have also been performed accounting for and ignoring electron energy losses in elastic electron–atomic collisions, $\overline{\nu V_\varepsilon}$ in (16). Accounting for these processes proved not to result in any noticeable changes.

4.2. The CCP behaviour at low currents

From figure 10 it is clearly seen that at small currents the EDF form is almost independent of current. If the EDF is determined mainly by the Joule heating in the plasma bulk, the scenario of maintenance of a CCP is practically the same as in the case of an ordinary dc positive column. The stationary condition demands the ambipolar lifetime to be equal to the inverse ionization frequency. Hence, in the plasma bulk the density profiles being similar to each other are proportional to j_0. The amplitude of the oscillatory field is proportional to $j_0/n(x)$ and does not change with current. Therefore, the EDFs are similar for small currents; the ionization rate is proportional to j_0. Since in the non-local approach the ionization in the sheaths is negligible [3], the ion flux is generated in the bulk plasma. Consequently, the ion flux to the surface is proportional to j_0, as well. The ion mobility for large E/p is proportional to $\sqrt{E/p}$, and the ion escape velocity at the electrode surface is proportional to $\sqrt{j_0}$. So the ion density at the electrode N_{sh} increases as $\sqrt{j_0}$, in contrast to the dependence $N_0 \sim j_0$ in the plasma bulk, and the oscillatory field in the sheath in plasma phase will grow with current as $j_0/N_{sh} \sim \sqrt{j_0}$.

To confirm the reasons proposed, the simulations without accounting for the Joule heating in the sheath were performed. Ignoring the sheath heating corresponds to $\tilde{E}(x) = 0$, $L_p < |x| < L_0$, when the electron energy diffusion coefficient is calculated. In figure 7 (dashed line), the resulting mean electron energy is presented. In figure 10 (dashed lines), the resulting EDFs are shown at the same currents as in the case for which the Joule heating was taken into account properly (figure 10, solid lines). The results demonstrate that in the absence of the sheath heating the EDF peak does not appear, the EDFs are similar to each other and $N_0 \sim j_0$, etc.

If the contribution of the Joule heating in the sheaths becomes considerable (N_0/N_{sh} increases with current), the above mentioned similarity, when all profiles are proportional to the central plasma density N_0, fails. For the results presented the similarity does not hold for $j_0 \sim$ 1 mA cm^{-2}.

4.3. EDF peak formation due to the non-locality

For large currents, when the ratio N_0/N_{sh} is great, the non-locality causes enrichment of the EDF by slow electrons.

In this case, the electrons can be separated into two groups. The electrons with $\varepsilon < e\Phi_{sheath} = e\Phi(L_p)$ are trapped in the region of the weak heating field ($\tilde{E}_0(x) \sim 1/n(x)$). The electrons with $\varepsilon > e\Phi_{sheath}$ can penetrate the sheath region where $\tilde{E}_0(x)$ is large. Hence, the $\overline{\nu D_\varepsilon}$ steeply rises with energy at $\varepsilon > e\Phi_{sheath}$ (see figures 11, 12). Because $\mathrm{d}f_0/\mathrm{d}\varepsilon = \Gamma_\varepsilon/\overline{\nu D_\varepsilon}$, where Γ_ε is the flux in energy space, the EDF slopes for $\varepsilon < e\Phi_{sheath}$ and $\varepsilon > e\Phi_{sheath}$ are strongly different. Roughly speaking, a two-temperature EDF appears (see also figure 1(c)).

The simulations demonstrating the described effect have been performed using both the local and the non-local approach. In figure 11 EDFs and electron energy diffusion coefficients are presented jointly. The simulations have been performed for helium. The parameters are the same as in the case presented in figure 7; j_0 = 8.8 mA cm^{-2}. For this current density the ion density profile is strongly inhomogeneous, the resulting ratio being $N_0/N_{sh} = 30$. The EDF corresponding to the local approach was calculated in the centre, using the value of the oscillatory field amplitude at the discharge centre $\tilde{E}(x = 0)$ (actually the EDF in uniform plasma with a given uniform electric field $\tilde{E}(x = 0)$ has been calculated, instead of the

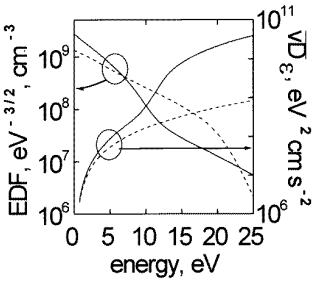

Figure 11. Results of the FM simulation; helium, p = 0.1 Torr, L_0 = 3.35 cm, ω = 13.56 MHz, j_0 = 8.8 mA cm^{-2}. Solid lines represent a non-local approach, dashed lines represent a local approach.

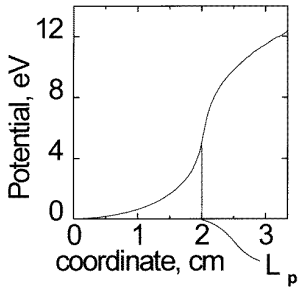

Figure 12. Calculated ambipolar potential. Under the same conditions as in figure 11, L_p represents a plasma–sheath boundary position.

whole profile $\tilde{E}(x)$ for the non-local approach). The non-local case is characterized by a steep growth of the $\overline{vD_\varepsilon}$ for energy $\varepsilon > e\Phi_{sheath} \sim 10$ eV (see figures 11, 12). In the local case this steep increase of $\overline{vD_\varepsilon}$ is missing. Accordingly, the low-energy peak of the EDF does not appear.

4.4. EDF evolution with pressure

The peaked EDF form due to the non-locality effect may not arise even when the plasma density profile is strongly inhomogeneous. In figure 13, the EDF evolution with varying pressure is demonstrated. Calculations were performed for $j_0 = 8.8$ mA cm^{-2} and $p = 0.03$–0.1 Torr. For $p = 0.03$ Torr the ratio $N_0/N_{sh} \sim 14$, but the mean electron energy is ~10 eV. The pressure decrease causes the EDF peak to disappear and mean energy to grow (see figure 14).

4.5. Comparison of the FM results with the experimental data in argon

As an illustration of the applicability of the FM method to different gases a comparison of the results of FM with the experimental data for argon has been performed. The domain of validity of the non-local approach is $pL_0 \lesssim$ 0.1 Torr cm.

The elastic electron–atomic collision cross-section is taken from [18]. Other cross-sections are based on data from [11]. In this simulation, electron–electron collisions were introduced which prove to be an important

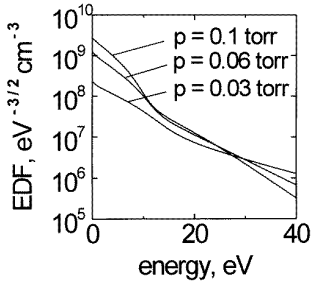

Figure 13. EDF evolution in He with pressure, for the same conditions as in figure 7; j_0 = 8.8 mA cm^{-2}.

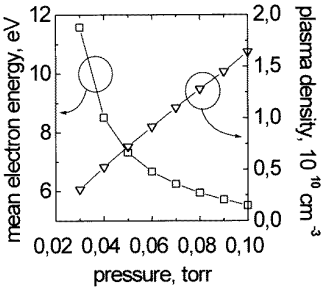

Figure 14. FM values of mean electron energy and plasma density in He versus pressure, for the same conditions as in figure 7, j_0 = 8.8 mA cm^{-2}.

mechanism of EDF formation under the used conditions. The right-hand side of electron kinetic equation (16) is to be supplemented by the corresponding spatially averaged electron–electron collision integral:

$$St_{ee}(F_0) = \frac{\mathrm{d}}{\mathrm{d}\varepsilon}\left(\overline{vD_\varepsilon}_{ee}\frac{dF_0}{\mathrm{d}\varepsilon} + \overline{vV_\varepsilon}_{ee}F_0\right) \tag{25}$$

$$(vV_\varepsilon)_{ee} = \frac{mv^3}{2n(x)}8\pi\nu_{ee}(v,x)\int_{e\phi(x)}^{\varepsilon}\mathrm{d}\varepsilon\frac{v}{m}F_0(\varepsilon)$$

$$(vD_\varepsilon)_{ee} = \frac{mv^3}{2n(x)}\frac{8\pi}{3}\nu_{ee}(v,x) \times\left[\int_{e\phi(x)}^{\varepsilon}\mathrm{d}\varepsilon\frac{v^3}{m}F_0(\varepsilon) + \frac{v^3}{m}\int_{\varepsilon}^{\infty}\mathrm{d}\varepsilon F_0(\varepsilon)\right]$$

where

$$\nu_{ee}(v,x) = \frac{4\pi e^4\Lambda_{ee}n(x)}{m^2v^3} \qquad v = \sqrt{(2/m)(\varepsilon - e\Phi(x))}$$

and Λ_{ee} is the Coulomb logarithm.

In figure 15, the evolutions of mean electron energy and ion density versus current density are plotted together. Solid and dashed lines correspond to the results obtained accounting for and ignoring electron–electron collisions, respectively. Experimental data are denoted by open triangles and squares. The discharge parameters are $p = 0.03$ Torr, $L_0 = 3.35$ cm, $\omega = 13.56$ MHz. Better qualitative agreement of the calculated mean electron energy with experimental data is obtained by accounting for electron–electron collisions. In this case the formation of EDFs with a peak is abrupt. The value of the current density, for which this transition occurs, corresponds to the experiment. Figure 16 depicts the discharge voltage. Accounting for electron–electron collisions

Table 1. Argon. The resulting values of the mean electron energy considering and ignoring the non-locality effect, the Ramsauer minimum, and the e–e collisions in the various combinations.

	Local case with the Ramsauer minimum (eV)	Non-local case without the Ramsauer minimum (eV)	Non-local case with the Ramsauer minimum (eV)
e–e collisions neglected	3.3	1	0.5
e–e collisions accounted for	3.49	2.56	1

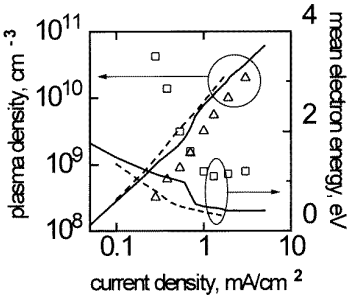

Figure 15. Argon, p = 0.03 Torr, L_0 = 3.35 cm, ω = 13.56 MHz. The mean electron energy, and plasma density evolution with current. Open squares and triangles represent experiment. Lines represent the FM results. The solid line represents data accounting for e–e collisions; the dashed line represents data ignoring e–e collisions.

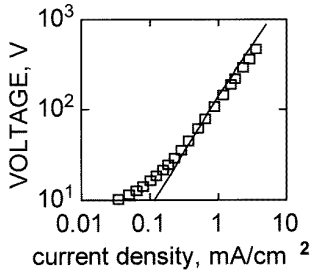

Figure 16. Argon, p = 0.03 Torr, L_0 = 3.35 cm, ω = 13.56 MHz. Discharge voltage versus current density. Open squares represent experiment. Solid line represents the FM results.

proves to be of no influence on the resulting discharge voltage. Quantitative agreement of the FM results with the experimental data is good for discharge voltage and satisfactory for plasma density, and the mean electron energy.

In section 5 it is demonstrated that the EDF form is sensitive to the details of the elementary processes. Moreover, the accuracy of the EDF calculation seems satisfactory in the case of the strongly peaked EDF (see 3.2). All these do not allow us to analyse quantitative agreement between experimental mean electron energy and the calculated one, as was performed for helium (see 4.1).

The importance of e–e collisions in Ar is related to the presence of the Ramsauer minimum in the electron–atomic elastic collision cross-section, that causes relatively small mean electron energy in comparison with that in He.

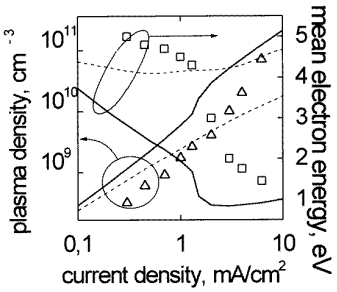

Figure 17. Argon, p = 0.1 Torr, L_0 = 3.35 cm, ω = 13.56 MHz. The mean electron energy, and plasma density evolution versus current density. Open triangles and squares represent experiment. Solid lines correspond to the FM results. Dashed lines correspond to the results of the FM performed ignoring the Joule heating in the sheath.

We also performed the simulations at $p = 0.1$ Torr. Under this condition the non-locality is not valid at the EDF tail. However, a reasonable agreement of the FM results with the experimental data has been obtained. The results of the simulations and the experimental data are presented in figure 17. In these simulations, an abrupt transition of the EDF to the peaked form is obtained. The current of the transition corresponds to the experiment. The e–e collisions seems to be the only mechanism to terminate the decreasing of the mean electron energy, as is the case for simulation performed at $p = 0.03$ Torr.

5. The sensitivity of the system to various processes

In order to investigate the effect of different mechanisms on the EDF formation in Ar, a series of EDF simulations has been performed. The EDFs were simulated considering and ignoring the non-locality effect, the Ramsauer minimum and the e–e collisions in the various combinations. The ion density profile was fixed and was previously obtained in the case of the fully self-consistent simulation taking into account all the mechanisms mentioned above. Neglecting the Ramsauer minimum corresponds to the assumption of constant electron–atomic elastic collision cross-section at $\varepsilon < 3$ eV—$\sigma_{ea}^{tr} = \sigma_{ea}^{tr}(3\text{ eV})$. The procedure of the simulation in the local approximation has been described above in section 4.3. Table 1 contains the resulting values of the mean electron energy.

The data obtained demonstrate that all the mechanisms are involved in the EDF formation. The temperature of the

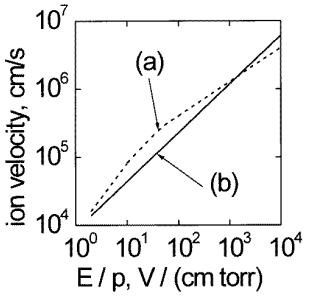

Figure 18. Ion velocities versus E/p. Dashed line represents the experimental data [11]. Solid line corresponds to the ion velocity obtained from (14).

Table 2. Results obtained accounting for different approximations ion velocities versus E/p.

	a	b	Experiment [6]
N_0	1.63×10^{10} cm^{-3}	5.82×10^{10} cm^{-3}	—
N_{sh}	5.75×10^{8} cm^{-3}	4.43×10^{8} cm^{-3}	—
$\langle\varepsilon\rangle$	5.52 eV	1.95 eV	1.4 eV

cold part of the EDF is very sensitive to the conditions used and to various assumptions.

Due to the self-consistent character of the problem, the EDF turns out to be very sensitive to the ratio of ion density in the discharge centre and in the accuracy of ion motion description. In the plasma it is determined by the small ambipolar field, and in the sheaths by the averaged strong space charge field. Accordingly, the widely used power approximation $u_i(E/p) \sim (E/p)^{1/(2+\beta)}$ (14) can cause significant errors, since this approximation is not valid for such a wide range of electric fields.

In figure 18 the ion velocities versus E/p in He are presented. The dashed line corresponds to the experiment (denoted as case (a)) [11]. The solid line corresponds to the case, when ion velocity was obtained from equation (14) (case (b)), for $\sigma_{ia} = 6.26\times10^{-15}(\varepsilon_{ion})^{-0.286}$ cm^{-2}. Here ε_{ion} is ion energy in eV. This expression fits the experimental data for the total ion–atomic cross-section (elastic collisions and charge exchange) [11] in a wide range of ion energies 5–400 eV. In this case, $u_i = 8.45\times10^3(E/p)^{0.714}$ cm s^{-1}, with E/p in V cm^{-1} Torr^{-1}. The range of E/p in figure 18 corresponds to the field variation obtained in the simulation data presented in figure 7, at $j_0 = 8.8$ mA cm^{-2}. It could be seen that the discrepancy between the (a) and (b) velocities attains approximately the value of 2 and is most pronounced at low E/p (for the ions at the discharge centre). Evidently, the simple power law form of u_i (E/p) is not applicable because of the extremely wide range of the field variation.

To show the importance of accurate calculations of ion velocity we have performed the test simulations using the different expressions for ion velocity at $j_0 = 8.8$ mA cm^{-2}. The results are given in table 2.

The calculations show that the power approximation for $u_i(E/p)$, (14), yields a significant increase in plasma density at the discharge centre. The reason is that the power approximation overestimates the ratio of the ion drift velocities and of densities in the sheath and in plasma. Therefore, the mean electron energy decreases in comparison to the realistic dependence (a). This decrease is additionally enhanced by increase of the relative contribution of the electron energy losses in the elastic collisions $\overline{vV\varepsilon}$ (17*b*).

Average electron energy losses consist of loss of $\cong \varepsilon^*$ in inelastic collisions, and of some additional loss of energy in the elastic collisions. The EDF tail, which determines the ionization rate, is relatively insensitive to the cross-section details, since the ionization rate is equal to the plasma diffusive losses. Accordingly, the power approximation (14) results in an increase of the fraction of cold electrons, and in further increase of the ion lifetime.

6. Conclusions and outlook

The agreement between the results obtained by FM and full-scale modelling demonstrates the validity of the FM method based on the non-local approach.

The results of the FM prove to be in good qualitative agreement with experimental data. The quantitative consistency of the values of the plasma density at the discharge centre and of the mean electron energy with the experimental values lies within a factor ~2. This accuracy can be regarded as quite satisfactory because of high sensitivity of the results to different processes and to the details of the cross-section description. Nevertheless, the discharge voltage proves to be not sensitive and can be calculated with good accuracy.

The system evolution with the current and pressure variation has been investigated. At low currents the evolution of EDF in a CCP is similar to the EDF evolution in a positive column. When the Joule heating in the discharge centre exceeds the heating in the sheath, the EDF form will not change with increasing current.

The role of the non-locality in the EDF peak formation is explained. The EDF peak due to the non-locality disappears with the decrease of current density and pressure.

At low pressures, $p < 0.1$ Torr, when the non-locality is valid, the low-energy EDF peak in He may exist only due to a non-locality effect. This will be the subject of further experimental investigations.

In argon, one of the important mechanisms of the EDF formation involves the e–e collisions. Accounting for the e–e collisions in helium did not cause noticeable changes.

The scenario of EDF transition to the form enriched by slow electrons is still unclear and possibly depends on the nature of the gas. It is the goal of further investigation. The research of the role of the collisionless heating is beyond the scope of the present paper and will be the aim of forthcoming work.

It can be stated that the FM provides all necessary information with reasonable accuracy in the range of parameters of interest for plasma processing: $\omega \sim 10$ MHz, 10^8 cm$^{-3} < n < 10^{11}$ cm^{-3}. The FM can be easily applied to two–three-dimensional systems, see e.g. [4]. It can be used in a wide range of pressures; for very low pressures accounting for the collisionless effects, as was done in

[13–15], is necessary. For pressures up to 200 mTorr–1 Torr some modifications in the calculation of the tail of the EDF, as in [24], are to be performed.

Acknowledgments

Stimulating discussions with A Bogaerts and R Gijbels are gratefully acknowledged. This work was partially supported by INTAS grant No 96-0235, RBRF grant for Support of International Collaboration N4391501, grant RBRF No 96-02-16918, grant RBRF No 98-02-16000, Naval Research Laboratory Contract N68171-97-M-5379, IAEA Contract No. 9238/R0/Regular Budget Fund, and partially sponsored by the University of Antwerp, Belgium (New Research Initiative Mathematical Simulation of Pulsed, Radio-Frequency and Magnetron Discharges).

References

[1] Lieberman M A and Lichtenberg A J 1994 *Principles of Plasma Discharges and Materials Processing* (New York: Wiley)
[2] Godyak V and Piejak R 1990 *Phys. Rev. Lett.* **65** 996–9
[3] Kaganovich I D and Tsendin L D 1992 *IEEE Trans. Plasma Sci.* **PS-20** 66–75
[4] Kortshagen U, Pukropskiy I and Tsendin L D 1995 *Phys. Rev.* E **51** 6063–77
[5] Behnke J, Golubovskiy Yu B, Nisimov S U and Porokhova I A 1996 *Contrib. Plasma Phys.* **6** 75–91
[6] Kaganovich I D and Tsendin L D 1992 *IEEE Trans. Plasma Sci.* **PS-20** 86–92
[7] Godyak V and Piejak R 1992 *Plasma Sources Sci. Technol.* **1** 36
Godyak V and Piejak R 1992 personal communication
[8] Smirnov A S and Tsendin L D 1991 *IEEE Trans. Plasma Sci.* **19** 130–40
[9] Gogyak V A and Sterberg N 1990 *Phys. Rev.* A **42** 2299–312
[10] Lieberman M A 1989 *IEEE Trans. Plasma Sci.* **PS-17** 338–41
[11] Raizer Yu P 1991 *Gas Discharge Physics* (Berlin: Springer)
[12] Velikhov E P, Kovalev A S and Rakhimov A T 1987 *Physical Phenomena in Gas Discharge Plasmas* (Moscow: Nauka) section 5.7 (in Russian)
[13] Aliev Yu M, Kaganovich I D and Schlüter H 1997 *Phys. Plasmas* **4** 2413–21
[14] Aliev Yu M, Kaganovich I D and Schlüter H 1998 *Proc. NATO ARW Electron Kinetics and Applications of Glow Discharges (St Petersburg, 1997)* ed U Kortshagen and L Tsendin (New York: Plenum)
[15] Buddemeier U and Kaganovich I D 1998 *Proc. NATO ARW Electron Kinetics and Applications of Glow Discharges (St Petersburg, 1997)* ed U Kortshagen and L Tsendin (New York: Plenum)
[16] Ivanov V V, Popov A M and Rakhimova T V 1995 *Phys. Plasma Rep.* **21** 692
[17] Surendra M, Graves D B and Morey I J 1990 *Appl. Phys. Lett.* **56** 1022–4
[18] Surendra M and Graves D B 1991 *Phys. Rev. Lett.* **66** 1469–72
[19] Wang Z, Lichtenberg A J and Cohen H 1998 *IEEE Trans. Plasma Sci.* **26** 59
[20] Dmitriev A P and Tsendin L D 1982 *Sov. Phys.–JETP* **54** 1071
[21] Golant V E, Zhilinsky A P and Sakharov I E 1980 *Fundamentals of Plasma Physics* (New York: Wiley)
[22] Tsendin L D 1977 *Sov. Phys.–JETP* **47** 925–8
[23] Godyak V A and Piejak R B 1993 *Appl. Phys. Lett.* **63** 3137–9
[24] Kolobov V I and Hitchon W N 1995 *Phys. Rev.* E **51** 280
[25] Yang Y and Wu H 1996 *J. Appl. Phys.* **80** 3699–704
[26] Godyak V A 1972 *Sov. Phys.–Tech. Phys.* **16** 1073
[27] Berezhnoi S V, Kaganovich I D and Tsendin L D 1996 *Appl. Phys. Lett.* **69** 2341
[28] Berezhnoi S V, Kaganovich I D, Levin E L and Tsendin L D 1994 *Proc. 10th Int. Conf. on Plasma Phys. (Foz do Iguacu, 1994)* vol 3, ed P H Sakanake, E D Besco and M V Alves (Brazil: National Institute of Space Research) pp 9–12
[29] Kortshagen U, Parker G J, and Lawler J E 1996 *Phys. Rev.* E **54** 6746
[30] Golubovskii Yu B, Nekuchaev V O, and Porokhova I A 1998 *Proc. NATO ARW Electron Kinetics and Applications of Glow Discharges (St Petersburg, 1997)* ed U Kortshagen and L Tsendin (New York: Plenum)